Journal of Solid State Chemistry 184 (2011) 2315–2321

Contents lists available at ScienceDirect

Journal of Solid State Chemistry

journal homepage: www.elsevier.com/locate/jssc

Local ordering and magnetism in $Ga_{0.9}Fe_{3.1}N$

Jens Burghaus [a,1], Moulay T. Sougrati [b,2], Anne Möchel [b,c,3], Andreas Houben [a,1], Raphaël P. Hermann [b,c,*], Richard Dronskowski [a,**]

[a] Institut für Anorganische Chemie, RWTH Aachen University, Landoltweg 1, D-52056 Aachen, Germany
[b] Faculty of Science, Université de Liège, B-4000 Liège, Belgium
[c] Jülich Centre for Neutron Science, JCNS, and Peter Grünberg Institut, PGI, JARA-FIT, Forschungszentrum Jülich, D-52425 Jülich, Germany

ARTICLE INFO

Article history:
Received 27 May 2011
Received in revised form
22 June 2011
Accepted 24 June 2011
Available online 2 July 2011

Keywords:
Nitride
Magnetism
Chemical synthesis
Mößbauer spectroscopy
Stoner criterion

ABSTRACT

Prior investigations of the ternary nitride series $Ga_{1-x}Fe_{3+x}N$ ($0 \le x \le 1$) have indicated a transition from ferromagnetic γ'-Fe_4N to antiferromagnetic "$GaFe_3N$". The ternary nitride "$GaFe_3N$" has been magnetically and spectroscopically reinvestigated in order to explore the weakening of the ferromagnetic interactions through the gradual incorporation of gallium into γ'-Fe_4N. A hysteretic loop at RT reveals the presence of a minority phase of only 0.1–0.2 at%, in accord with the sound two-step synthesis. The composition of the gallium-richest phase "$GaFe_3N$" was clarified by Prompt Gamma-ray Activation Analysis and leads to the berthollide formula $Ga_{0.91(1)}Fe_{3.09(10)}N_{1.05(7)}$. Magnetic measurements indicate a transition around 8 K, further supported by Mössbauer spectral data. The weakening of the ferromagnetic coupling through an increasing gallium concentration is explained by a simple Stoner argument. In $Ga_{0.9}Fe_{3.1}N$, the presence of iron on the gallium site affects the magnetism by the formation of 13-atom iron clusters.

1. Introduction

The archetypal phase γ'-Fe_4N (space group $Pm\bar{3}m$, a=3.8009 (1) Å) [1] has been intensively studied by experimental and theoretical investigations. It is characterized by a large saturation magnetization of 208 emu g^{-1} [2] being close to that of α-Fe (218 emu g^{-1}). Furthermore, a low coercivity (H_C=5.8 Oe ≈ 460 A m^{-1}) [3] in combination with a high chemical inertness makes it a promising candidate for high-density magnetic storage [4–6].

Interestingly enough, the successive substitution of the iron atoms on the Wyckoff site 1*a* by gallium changes the magnetic properties significantly, and one finds a decrease of the coercivity and a degradation of the ferromagnetic coupling [7,8], which is out of the ordinary for most of the reported ternary nitrides [9]. The final product of elemental substitution, "$GaFe_3N$", also crystallizes in space group $Pm\bar{3}m$ with a similar lattice parameter of a=3.8001(1) Å. Here, gallium exclusively occupies Wyckoff position 1*a* (Fig. 1). This can be explained, first, by the greater strength of the Fe–N bond compared to Ga–N [8]. Another reason lies in the larger metallic radius of gallium (r_M(Ga)=1.41 Å) [10] compared to the one of iron (r_M(Fe)=1.24 Å) [10] because the coordination sphere of the cuboctahedron around 1*a* (1.42 Å) is also significantly larger than the one around 3*c* (1.28 Å). Thus, the 1*a* position is favored by gallium [4], in good accord with a theoretical estimate of the atomic ordering [8].

2. Results and discussion

2.1. Synthesis

Practically phase-pure "$GaFe_3N$" was synthesized by the recently introduced two-step ammonolysis reaction starting from powdered Ga_2O_3 and Fe_2O_3; so far, this route exclusively avoids the formation of a GaN by-product [8]. The optimized synthesis uses a high sintering-temperature step (1100 °C, 1 min) and a subsequent nitridation reaction (530 °C, 3 h). The ammonolysis gas was a NH_3:H_2 mixture with a 1:1 ratio.

2.2. Hysteretic loop at room temperature

In order to ultimately analyze the chemical purity of the crystallographically phase-pure product, hysteretic loops of the magnetic susceptibility were measured at 8 and 300 K using

* Corresponding author at: Jülich Centre for Neutron Science, JCNS, and Peter Grünberg Institut, PGI, JARA-FIT, Forschungszentrum Jülich, D-52425 Jülich, Germany. Fax: +49 2461 61 2610.
** Corresponding author. Fax: +49 241 80 92642.
E-mail addresses: moulay-tahar.sougrati@univ-montp2.fr (M.T. Sougrati), r.hermann@fz-juelich.de (R.P. Hermann), drons@HAL9000.ac.rwth-aachen.de (R. Dronskowski).
[1] Fax: +49 241 80 92642.
[2] Present address: Université Montpellier 2, Institut Charles Gerhardt (UMR 5253) Case courrier 00004, Place Eugène Bataillon, 34095 Montpellier Cedex 5, France. Fax: +33 4 67 14 38 62.
[3] Fax: +49 2461 61 2610.

0022-4596/$ - see front matter © 2011 Elsevier Inc. All rights reserved.
doi:10.1016/j.jssc.2011.06.031

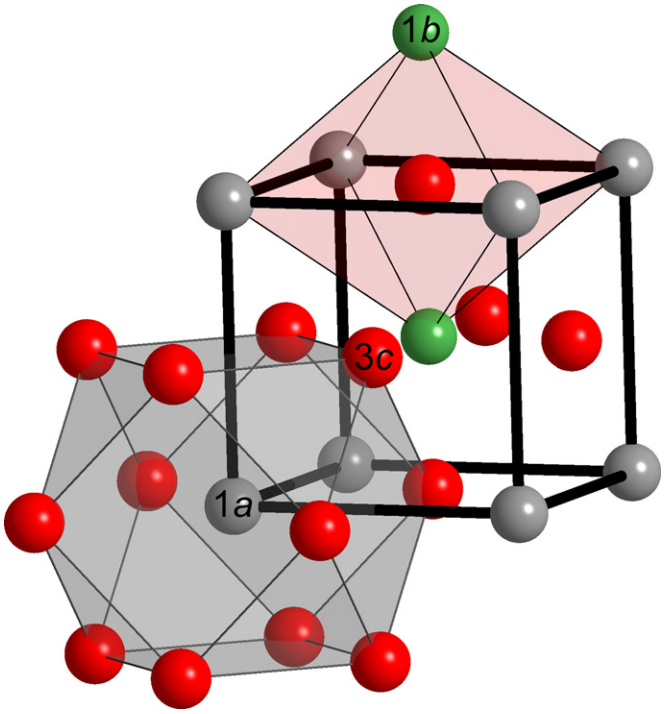

Fig. 1. The crystal structure of $GaFe_3N$ in space group $Pm\bar{3}m$ ($a=3.8001(1)$ Å). The nitrogen atom (green) occupies the very center (Wyckoff position 1*b*), the iron atoms (red) are found at the face centers (3*c*), and the gallium atoms are at the corner position (1*a*). The iron atoms are octahedrally coordinated by gallium and nitrogen atoms whereas gallium experiences a cuboctahedral iron coordination. (For interpretation of the references to color in this figure legend, the reader is referred to the web version of this article.)

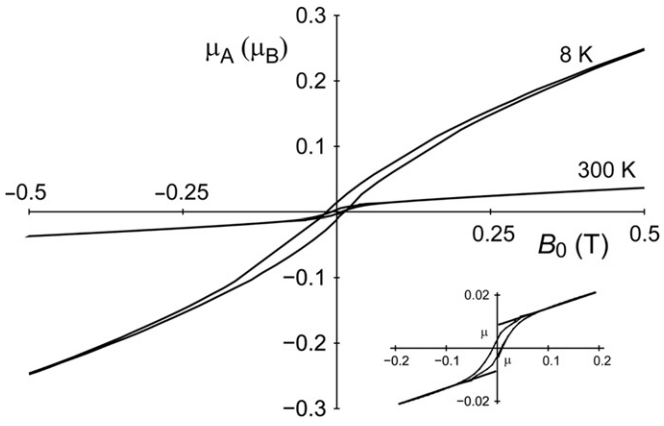

Fig. 2. *Main plot:* hysteretic loops of $Ga_{0.9}Fe_{3.1}N$ at 8 and 300 K. The small hysteresis for 300 K evidences the formation of a very small amount of a ferromagnetic side-phase. *Inset*: calculation of the side-phase amount through the intercept of the magnetization axis.

a PPMS (Quantum Design) magnetometer at applied fields H between -0.5 and $+0.5$ T (see Fig. 2). Up to the largest applied field, the magnetization of the sample stays unsaturated. More importantly, there exists a very small hysteresis even at 300 K, which suggests the formation of a minor side-phase during synthesis; note that 300 K is already in the paramagnetic range of "$GaFe_3N$". We may therefore estimate the amount of the most probable side-phases γ'-Fe_4N and/or α-Fe since both have a magnetic saturation moment of ca. 2.2 μ_B per Fe atom. Therefore, the amount of γ'-Fe_4N (or α-Fe) is equal to (X-ray invisible) 0.1–0.2 at%, which evidences the exceedingly good quality of the two-step ammonolysis.

2.3. Prompt Gamma-Ray Activation Analysis (PGAA)

In analogy to prior investigations on "$GaFe_3N$" [7,8], the occupation of the 1*a* position with either gallium and/or iron deserves closer attention. First, it is rather challenging to refine the gallium occupation using the Rietveld method because the Ga and Fe X-ray form factors are quite close to each other. Second, the nitrogen concentration is also of high interest despite the fact that the occupation factor of such light element is hardly refinable from powder XRD data.

Thus, Prompt Gamma-Ray Activation Analysis (PGAA) measurements [11] were performed at the research reactor FRM II in Garching close to Munich in order to determine the bulk elemental composition. The sample was measured with a standard PGAA setup, and the results of the analysis are shown in Table 1. It is intrinsic to this method that, despite using a standard, only *relative* compositions can be determined by comparing the integrated peak areas related to different isotopes. Assuming that the 3*c* position of the $Pm\bar{3}m$ space group is fully occupied by iron and that the 1*a* position has a full but mixed occupation by iron and gallium, the following equation holds for their occupation factors x: ${}^{1a}x^{Ga}+{}^{1a}x^{Fe}+{}^{3c}3^{Fe}=4$. Assuming the absence of metal vacancies, the renormalized PGAA results then yield the composition $Ga_{0.91(1)}Fe_{3.09(10)}N_{1.05(7)}$.

This finding is in agreement with the already derived gallium occupation of Wyckoff position 1*a*, namely 82(6)%, by a Rietveld refinement and 90(10)% using SEM/EDX, both for $Ga_{0.9}Fe_{3.1}N$ [7,8]. Thus, PGAA gives essentially the same gallium occupation of 91(1)% but with a significantly smaller error bar. While the occupation of the metal atoms, especially for $Ga_{0.9}Fe_{3.1}N$, has been well studied, investigations on the nitrogen content are usually neglected for $M_{1-x}Fe_{3+x}N$ phases due to obvious reasons. The present PGAA results clearly show that the nitrogen content is one for $Ga_{0.9}Fe_{3.1}N$, and position 1*b* is fully occupied by nitrogen.

2.4. Alternating Current Magnetic Susceptibility (ACMS) measurements

Alternating Current Magnetic Susceptibility (ACMS) measurements were performed to analyze the magnetic properties of $Ga_{0.9}Fe_{3.1}N$ (see Fig. 3) in more detail. The sample was subjected to an applied field of 300 Oe with a frequency of 10 kHz. The data evidence a minimum of the inverse molar susceptibility χ_m^{-1} around 8 K, suggestive of a magnetic transition that correlates with the Mössbauer spectral results (see below). The latter reveals a coupling of the isolated Fe_0(3*c*) atoms (Fe on 3*c* with 0 Fe near neighbors) at 5 K, as also discussed below.

To study the occupation of Ga and Fe on the 1*a* and 3*c* sites and, more importantly, their local magnetic ordering, ^{57}Fe Mössbauer spectroscopy was carried out. Beforehand, we will discuss further details of the crystal structure needed for the proper interpretation of these Mössbauer data.

2.5. Structure

As already mentioned, the crystal structure of $Ga_{0.9}Fe_{3.1}N$ contains two crystallographically distinguishable metal sites: the

Table 1
Results of PGAA measurements obtained at the FRM II. Given are the fitted areas of the PGAA spectra and resulting intensities, corrected by the capture cross section [11] of the specific element and the detector sensitivity. Assuming full occupation (Ga+Fe=4), this gives the formula $Ga_{0.91(1)}Fe_{3.09(10)}N_{1.05(7)}$.

Element	Area	Intensity (barn)
Ga	0.905(11)	$7.30(9)\times10^4$
Fe	0.779(25)	$2.49(8)\times10^5$
N	0.095(6)	$8.42(8)\times10^4$

3*c* site is located at the face centers and is fully occupied by iron whereas the 1*a* corner site is fully occupied by gallium and a small amount of iron atoms (Fig. 1). In addition, the 1*b* site is occupied by N. The local symmetry of the 1*a* site is cubic and conforms to point-group symmetry O_h, whereas the 3*c* site has only one 4-fold rotation axis and D_{4h} symmetry. Consequently, for the analysis of the Mössbauer spectra the quadrupole splitting for the 1*a* site can be constrained to zero (cubic symmetry for all spectra) but it is entirely free for the 3*c* site. Nominally, the Ga atom on 1*a* has twelve nearest Fe(3*c*) neighbors while the Fe atom on 3*c* has two N(1*b*) and four Ga(1*a*) nearest neighbors (Fig. 1). Due to site disorder, however, a few 1*a* sites are occupied by Fe instead of Ga. The crystal-chemical formula can thus be written as $^{1a}[Ga_{(1-x)}Fe_x]^{3c}[Fe_3]^{1b}N$ if we assume that there are no 1*a* and 3*c* vacancies. It is likely that the two metals are randomly distributed on the 1*a* site, which also admits the presence of a few close Fe(1*a*)–Fe(1*a*) contacts.

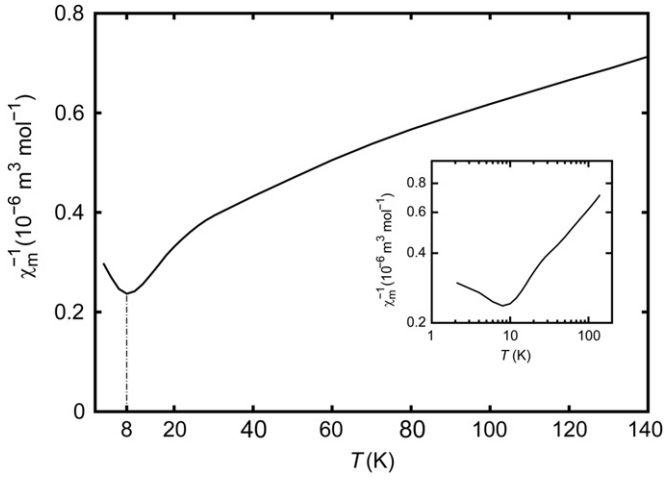

Fig. 3. *Top:* reciprocal magnetic susceptibility χ_m^{-1} for $Ga_{0.9}Fe_{3.1}N$ at an applied field of 300 Oe and applied frequency of 10 kHz as a function of the temperature *T*. The minimum is found at 8 K. The inset shows the same reciprocal magnetic susceptibility but using a logarithmic temperature scale.

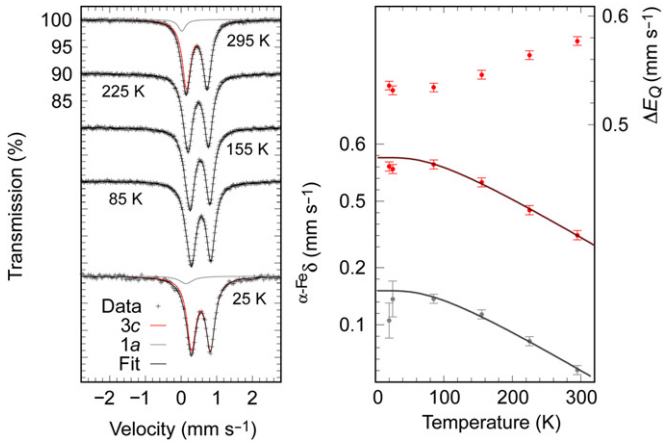

Fig. 4. Mössbauer spectra for $Ga_{0.9}Fe_{3.1}N$ between 85 and 295 K (left) and temperature dependence of the quadrupole splitting and isomer shift relative to α-Fe (right).

2.6. Mössbauer spectra, model, results, and discussion

The ^{57}Fe Mössbauer spectra of $Ga_{0.9}Fe_{3.1}N$ reveal that between 20 and 300 K this material is paramagnetic, and magnetic hyperfine splitting is observed only below 20 K. The paramagnetic spectra obtained between 295 and 25 K are depicted in the left panel of Fig. 4 and have been analyzed by a simple model comprised of a doublet for the Fe(3*c*) component and a singlet for the Fe(1*a*) component. For clarity, the individual components are only shown for 25 and 295 K. The quadrupole splitting, ΔE_Q, of the Fe(3*c*) component and the isomer shifts, δ, of both components are found in the right panel of Fig. 4. The line width, Γ, for both components is rather narrow, that is, between 0.25 and 0.3 mm s^{-1}, except at 25 and 20 K where a broadening up to 0.5 mm s^{-1} of the Fe(1*a*) component is observed. As the data were measured in two separate runs, the value for the isomer shifts at and below 25 K is slightly smaller, probably due to a small systematic error in the order of 0.01 mm s^{-1}. The Mössbauer spectral parameters for these spectra are summarized in Table 2.

The analysis of the paramagnetic spectra reveals a normal temperature dependence of the isomer shift, which has been fitted with the Debye model for the second-order Doppler shift. The obtained overall Lamb–Mössbauer temperature is $\Theta_{LM}^{SOD}=370(20)$ K, which is in good agreement with a similar analysis (not shown) of the temperature dependence of the total spectral area, revealing a Lamb–Mössbauer temperature of $\Theta_{LM}^{A}=395(10)$ K. If analyzed separately, a Lamb–Mössbauer temperature of 410(40) K is obtained for the Fe(1*a*) site, indicating a slightly stronger bonding to its near iron neighbors. For Fe(3*c*), ΔE_Q exhibits a small temperature dependence, with an almost linear increase of the absolute value, and the obtained value of ≈ 0.55 mm s^{-1} is close to 0.526 mm s^{-1} as observed for the Fe(3*c*) doublet in the paramagnetic spectrum of γ'-Fe_4N by Bartels and Becker [12]. The observed room-temperature isomer shifts, 0.441(5) and 0.021(5) for Fe(3*c*) and Fe(1*a*), respectively, deviate from those in γ'-Fe_4N, which are 0.313 and 0.241, respectively. In particular, the difference in isomer shift between the Fe(3*c*) and Fe(1*a*) site is much larger in this compound than in γ'-Fe_4N or in $RhFe_3N$ [13]. We thus also tried an alternative fitting of the paramagnetic spectra with a smaller difference in isomer shifts between both sites. Although good individual fits were obtained, the overall deviations came out larger than in the here reported model, which is also more consistent with the analysis of the low-temperature magnetic spectra.

Because of the mixed Ga and Fe occupation of the 1*a* site, there is not only a 1*a* Mössbauer spectral component but also different local environments for the iron on the 3*c* site, which must be taken into account. A common approach, which relies on a random site occupation with a given probability, is to model the

Table 2
Mössbauer spectral parameters for the non-magnetically split spectra in Figs. 4 and 5 together with χ^2_{red}, the reduced sum of the squared residuals for the fits.

T (K)	Γ(Fe(3*c*)) (mm s^{-1})	δ(Fe(3*c*)) (mm s^{-1})	ΔE_Q(Fe(3*c*)) (mm s^{-1})	*r*(Fe(1*a*)) (%)	Γ(Fe(1*a*)) (mm s^{-1})	δ(Fe(1*a*)) (mm s^{-1})	χ^2_{red}
295	0.286(2)	0.441(5)	0.577(5)	7(1)	0.25(1)	0.021(5)	1.3
225	0.289(2)	0.484(5)	0.564(5)	7(1)	0.26(2)	0.071(5)	1.4
155	0.291(2)	0.533(5)	0.546(5)	9(1)	0.28(1)	0.118(5)	1.4
85	0.294(2)	0.564(5)	0.534(5)	8(1)	0.27(1)	0.146(5)	1.2
25	0.310(4)	0.556(5)	0.532(5)	7(1)	0.44(6)	0.15(3)	1.1
20	0.326(4)	0.561(5)	0.536(5)	9(1)	0.57(6)	0.11(3)	1.2

spectra with a binomial distribution of spectral parameters [14]. As the paramagnetic spectra are quite simple and readily analyzed with a simple two-component model, we proceeded with the binomial analysis only for the magnetic spectra, for which the simple models fail (see below). A correlated distribution of isomer shift and quadrupole splitting for the binomial terms in the paramagnetic spectra is likely but the data did not allow for a reliable extraction of this distribution.

A first estimate for x, the Fe occupation on the 1a site, can be obtained from the relative spectral area r of the Fe(1a) component in the paramagnetic spectra. We observed $r=0.075(5)$ and, accordingly (see below), $x=3r/(1-r)\approx 0.25(2)$. Note, however, that the absorption in these paramagnetic spectra is somewhat large at $\approx 15\%$, and therefore the quantities obtained directly from the spectral areas, including Θ_{LM}^{A}, should be considered with a little caution as we did not carry out transmission integral corrections.

Below 20 K, a gradual magnetic splitting of the spectra is observed upon cooling, and at 5 K the spectrum exhibits a complex shape. Attempts to model this spectrum with a simple two magnetic component model as above or by supposing dynamic effects and magnetic relaxation failed. The next degree of complexity requires to jointly consider the local magnetic interactions and the atomic neighbors. In a first approximation, neglecting the second-nearest-neighbor environment, the Mössbauer spectra should be decomposed in one sub-spectrum, with a relative area R_{1a} associated to the iron located on 1a, and five sub-spectra associated to iron on 3c that have between zero and four Ga nearest neighbors substituted by Fe. Their relative areas R_i are given by the binomial distribution:

$$R_i=[4!x^i(1-x)^{4-i}]/(i!(4-i)!),$$

where $i=0,\ldots,4$ is the number of nearest Fe(1a) neighbors for a given 3c site, and x is the Fe concentration on 1a. Considering that $R_{1a}=x$, the total spectral area A is proportional to $A=x+3\sum_i R_i=3+x$. Consequently, this model yields two ways to obtain the site disorder x, namely, first by considering the ratio r of the A_{1a} spectral area to the total area, as done above for the paramagnetic spectra, and, second, by considering the ratio of A_i spectral areas with different i. Because Rietveld refinement, PGAA, AAS, and EDX let us expect $0<x<0.2$, we can neglect the A_3 and A_4 spectral contributions that correspond to less than 2.5% of the total spectral area. We therefore group the contributions for two and more ^{1a}Fe nearest neighbors in a "2+" sub-spectrum. Because the relative area of Fe(1a) is also quite small, $r=R_{1a}/A=x/(3+x)<6.25\%$, we cannot expect to reliably obtain x from the first approach and, consequently, we constrained the binomial "x" and the spectral area "x" to be the same in all fits for the magnetic spectra. The nearest-neighbor environment also allows one to preliminarily assign the spectral component with the largest hyperfine field to Fe(1a), with twelve potentially magnetic iron nearest-neighbors building up a Fe_{13} magnetic cluster, and the spectral components with smaller hyperfine fields to Fe(3c) with only at most four Fe nearest neighbors.

The final fitting model on which Fig. 5 relies used a reduced number of fit parameters: for Fe(1a), the isomer shift, hyperfine field, H, line width, and the spectral area cross-constrained to the binomial distribution; for the three Fe_i(3c) sub-spectra with $i=0$, 1 and "2+" Fe near neighbors, three hyperfine fields, two quadrupole interactions for the paramagnetic and magnetic component (see below), one single isomer shift, and one line width per component mimicking slight field distributions. The relative spectral areas were constrained to the binomial model described above. From preliminary fits we found $x=0.17(2)$ and constrained the binomial distribution to this x value for the final fits; we further constrained the isomer shift for Fe(1a) to 0.15 mm s^{-1}, in agreement with the extrapolation from the paramagnetic spectra. These preliminary fits also indicate that, except at 5 K, the Fe$_0$(3c) component is paramagnetic with $\Delta E_Q=0.54(1)$ mm s^{-1}. Attempts to fit the Fe$_0$(3c) sub-spectrum at 11 and 15 K with a magnetic component with ΔE_Q constrained to this value and with a free angle θ between the electric field gradient tensor and the magnetic quantization axes were not successful. The Fe$_0$(3c) atoms begin to order magnetically at 5 K (likely below 8 K, which corresponds to the ACMS measurements, discussed above), indicating the onset of percolation or a Ruderman–Kittel–Kasuya–Yosida (RKKY) type interaction.

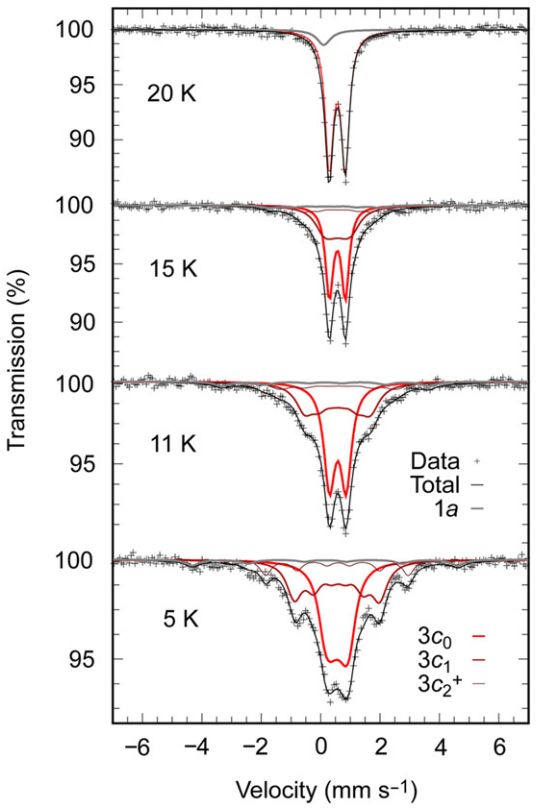

Fig. 5. Mössbauer spectra for $Ga_{0.9}Fe_{3.1}N$ between 20 and 5 K, with the subcomponents for the binomial distribution analysis, see also text.

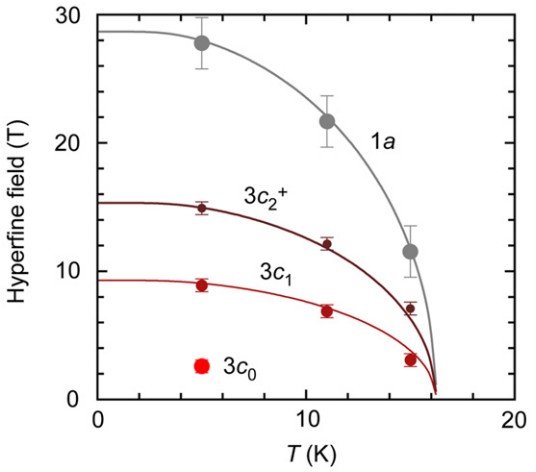

Fig. 6. Temperature dependence of the hyperfine field for the different sites and local environment configurations. Atom Fe$_0$(3c) exhibits a measurable field only at 5 K. The solid lines are a guide for the eye and correspond to the mean-field behavior with $T_C=16.3(5)$ K and $\mu=2.2\ \mu_B$.

Table 3
The Mössbauer spectral parameters for the magnetically split spectra in Fig. 5 and χ^2_{red}, the reduced sum of the squared residuals for the fits. The quadrupole shift for the magnetically split components are all very small, −0.02(2) mm s^{-1}; the relative areas of the Fe$_0$(3*c*):Fe$_1$(3*c*):Fe$_{2+}$(3*c*):Fe(1*a*) components have been cross-constrained for a simultaneous fit at three temperatures that yield the ratios 0.464:0.371:0.111:0.054, see text; (–) indicate constrained parameters, see text.

T (K)	δ[Fe(3*c*)] (mm s^{-1})	Γ[Fe$_0$(3*c*)] (mm s^{-1})	ΔE_Q[Fe$_0$(3*c*)] (mm s^{-1})	H[Fe$_0$(3*c*)] (T)	Γ[Fe$_1$(3*c*)] (mm s^{-1})	H[Fe$_1$(3*c*)] (T)	Γ[Fe$_{2+}$(3*c*)] (mm s^{-1})	H[Fe$_{2+}$(3*c*)] (T)	Γ[Fe(1*a*)] (mm s^{-1})	δ[Fe(1*a*)] (mm s^{-1})	H[Fe(1*a*)] (T)	χ^2_{red}
15	0.562(2)	0.31(1)	0.532(5)	–	0.71(6)	3.1(1)	0.6(1)	7.1(4)	0.61(–)	0.15(–)	11.5(7)	1.0
11	0.577(3)	0.45(1)	0.554(5)	–	0.72(4)	6.9(1)	0.8(1)	12.1(4)	0.61(–)	0.15(–)	21.7(5)	1.1
5	0.571(4)	0.55(2)	–	2.6(1)	0.62(3)	8.9(1)	0.43(3)	14.9(1)	0.54(8)	0.15(–)	27.8(3)	1.5

The fits yield a 0.57(1) mm s^{-1} isomer shift for the Fe(3*c*) components, and a quadrupole shift of –0.02(2) mm s^{-1} for all Fe(3*c*) magnetic components. The hyperfine field gradually evolves for Fe$_1$(3*c*), Fe$_{2+}$(3*c*), and Fe(1*a*), as shown in Fig. 6. From the temperature variation of the hyperfine fields we estimate a critical temperature for the appearance of local magnetic order of T_C=16.3(5) K. For comparison, the hyperfine field variation in the mean-field approximation obtained by solving the Brillouin equation, and assuming a metal-like 2.2 μ_B moment for Fe, is shown for all sites. The line widths are $\approx$0.6(1) mm s^{-1} for the magnetic components and gradually increase from 0.3 to 0.55 mm s^{-1} for the Fe$_0$(3*c*) component upon cooling from 20 to 5 K. The Mössbauer spectral parameters for these spectra are summarized in Table 3.

As alluded to earlier and shown by Mössbauer spectroscopy and PGAA, the Wyckoff 1*a* site is not exclusively occupied by gallium. Mössbauer spectroscopy indicates that the local magnetic moments of the Fe(1*a*) atoms likely affect the Fe(3*c*) atoms; there will be, once in a while, magnetic Fe$_{13}$ clusters from twelve Fe(3*c*) atoms around one Fe(1*a*) atom (Fig. 1). As a rule of thumb for itinerant magnetism, a hyperfine field of 15 T corresponds to a magnetic moment of approximately 1 μ_B [15]. The hyperfine field on the Fe(1*a*) site is about 30 T (see Fig. 6), which corresponds to a magnetic moment of $\approx$2 μ_B, whereas the magnetic moment on the Fe$_{2+}$(3*c*) is determined as $\approx$1 μ_B; for the Fe$_1$(3*c*) atom, one finds $\approx$0.6 μ_B. We stress the fact that the iron sites 1*a* and 3*c* have different local magnetic moments.

The local magnetic moments can also be calculated on the basis of density-functional theory. An eight times enlarged super-cell with the composition $Ga_{0.875}Fe_{3.125}N$ and a ferromagnetic ground state was constructed such that the 1*a* site contained seven gallium atoms and one iron atom. The 3*c* site was fully occupied by iron. With respect to the composition $Ga_{0.875}Fe_{3.125}N$ and space group $Pm\bar{3}m$, only one Ga/Fe arrangement on the 1*a* site is possible. In the self-consistent state, the local magnetic moments of Ga(1*a*) and N(1*b*) are practically zero, as expected. Nonetheless, the moment of the Fe(1*a*) atom arrives at $\approx$2.9 μ_B, larger by about 1 μ_B than the one of the Fe(3*c*) atom ($\mu_a \approx 1.8\ \mu_B$). This is well explainable by the influence of the neighboring nitrogen atom and its strongly covalent bond, as is also known from γ'-Fe_4N [16], which exhibits similar theoretical magnetic moments [17]. Although the calculated moments are larger than those from the Mössbauer analysis, the trend is correctly reproduced. Compared to α-Fe with a local moment of 2.2 μ_B (or $\approx$33 T), the Fe(1*a*) atoms have a quite similar local moment of 30 T (or $\approx$2.0 μ_B), which is reasonable considering the surrounding by twelve Fe(3*c*) atoms. Thus, Fe$_{13}$ metallic clusters are formed for every Fe(1*a*). An aggregation of clusters by sharing common Fe(3c) atoms is possible.

In comparison to the already published results of $RhFe_3N$ and other ternary nitrides with the composition MFe_3N, and *M* being a transition metal, the magnetic properties of $Ga_{0.9}Fe_{3.1}N$ are remarkable. Since almost all known ternary nitrides are ferromagnetic, one may ask for the role of gallium with respect to the "dilution" of the magnetism, in particular concerning its influence on the surrounding Fe(3*c*) atom. One may, for example, consider the simple Stoner model [18,19] for itinerant magnetism. The Stoner criterion [20,21] is a (semi-)quantitative argument for the existence of ferromagnetism of transition metals, stating that large electronic densities-of-states at the Fermi level (ε_F), together with a strong exchange interaction, are necessary to obtain ferromagnetism. Starting with γ'-Fe_4N, gallium atoms were successively incorporated into its crystal structure on the Wyckoff 1*a* site, that is, in the first coordination sphere of Fe(3*c*). A super-cell with three different compositions of $^{1a}[Ga_{(1-x)}Fe_x]^{3c}[Fe_3]^{1b}N$ (x=1,

Table 4
Number of states at the Fermi level $N(\varepsilon_F)$ belonging to a single Fe(3*c*) atom, obtained from non-spin polarized LMTO-GGA calculations.

x	$N(\varepsilon_F)$ of Fe(3*c*)
1	2.0
1/2	1.6
0	1.4

1/2, 0) was iterated towards self-consistency but using a non-spin-polarized electronic structure.

As shown in Table 4, the number of states at the Fermi level, $N(\varepsilon_F)$, belonging to the Fe(3*c*) atom, decreases significantly while more Ga(1*a*) atoms appear close to the Fe(3*c*) atom. This observation supports the idea of a weakening ferromagnetism with an increase in gallium concentration. This finding is in accord with earlier experimental results, e.g. with the decrease of the magnetic saturation moment [7,8].

Overall, the magnetism in this compound can be understood as a kind of "cluster magnetism" where Fe clusters are incorporated in a metallic matrix of gallium. This idea is reminiscent of similar observations within face-centered cubic (fcc) iron clusters in fcc-type Rh, Pd, and Ag [22]. There is a correlation between the iron cluster size in the underlying metallic matrix of 4*d* metals and the occurrence of different magnetic orderings. Fe in Ag shows antiferromagnetism for clusters of 24 atoms, whereas Fe in Pd reveals a change of magnetic ordering for clusters as large as 42 atoms. In comparison, $Ga_{0.9}Fe_{3.1}N$ reveals ferromagnetism for clusters of 13 atoms.

3. Conclusion

The combined analytical techniques herein corroborate the almost phase-pure quality of "$GaFe_3N$" based on the two-step ammonolysis route. The use of Prompt Gamma-ray Activation Analysis (PGAA) results in a composition of $Ga_{0.91(1)}Fe_{3.09(10)}N_{1.05(7)}$, in excellent agreement with previous results [7,8]. ACMS measurements reveal a magnetic ordering of the Fe_0(3*c*) atoms around 8 K, which correlates with the Mössbauer spectral results (5 K) and is explained by an onset of percolation or a RKKY type interaction. Furthermore, a critical temperature of 16.3(5) K is estimated for the appearance of a local magnetic ordering for the interactions between $Fe_{\neq 0}$(3*c*) and Fe(1*a*) atoms. Since $Ga_{0.9}Fe_{3.1}N$ is berthollide, such 1*a* iron atoms are surrounded by twelve adjacent $Fe_{\neq 0}$(3*c*) atoms, thereby building up Fe_{13} clusters. Thus, the decrease of the magnetic saturation moment with an increase of the gallium concentration within the $Ga_{1-x}Fe_{3+x}N$ system is not necessarily linked to a change from ferromagnetic to an *antiferromagnetic* ordering within the non-stoichiometric $Ga_{0.9}Fe_{3.1}N$, as assumed in prior publications [7,8].

The change of the magnetism upon going from γ'-Fe_4N to $Ga_{0.9}Fe_{3.1}N$ through gallium incorporation can be described as a dilution of the ferromagnetic interactions. This circumstance is mirrored by a decrease in the number of Fe(3*c*) atomic states at the Fermi level. Nevertheless, different neutron experiments are required to validate the existence of iron clusters and to furthermore determine their exact size.

4. Experimental section

Mössbauer spectroscopy: The Mössbauer spectra were measured in two runs, first between 5 and 25 K with a velocity range of ± 12 mm s^{-1}, and second between 85 and 295 K with a velocity range of ± 4 mm s^{-1}. The constant-acceleration spectrometer utilized a rhodium-matrix ^{57}Co source and was calibrated with α-Fe powder at room temperature. The Mössbauer spectra were obtained in a Janis Supervaritemp cryostat, and the absorber contained 25 mg cm^{-2} of the powdered sample mixed with boron nitride.

PGAA (Prompt Gamma-Ray Activation Analysis) was performed at the research reactor Forschungsneutronenquelle Heinz Maier-Leibnitz (FRM II) in Garching. A white cold neutron beam with an average wavelength of 6.7 Å was used. Data acquisition was done by two standard Compton-suppressed gamma spectrometers, namely a HPGe detector with relative efficiency of 60% (ORTEC poptop) inserted in annulus BGO scintillators (coaxial geometry) and an HPGe detector with relative efficiency of 36% surrounded by a NaI(Tl)/BGO scintillation system (perpendicular geometry). The sample chamber was evacuated in order to suppress the gamma-ray background coming from the neutron capture on air, which is especially important for the detection of nitrogen within the sample. The acquisition time of the $Ga_{0.9}Fe_{3.1}N$ sample was 25,388 s, whereas the acquisition time of the background was 37,988 s.

PPMS: Hysteretic loops were recorded at a temperature of 8 K and room temperature in the field range ± 1 T by PPMS magnetometry (Quantum Design). Temperature-dependent measurements were carried out using an Alternating Current Magnetometer (ACMS) in the temperature range 2–200 K at an applied field of 300 Oe and an applied frequency of 10,000 Hz.

Computational details: The Tight-Binding Linear Muffin-Tin Orbital (TB-LMTO) method [23] was used by employing the Perdew–Wang non-local generalized-gradient approximation (GGA) [27], as implemented in the LMTO code to calculate electron densities at the Fermi level from lowest-energy structures. These calculations were performed with the Linear Muffin-Tin Orbital theory [24], which represents a fast, linearized form of the KKR method [25,26]. The TB-LMTO calculations were carried out within the Atomic Spheres Approximation (ASA) [23,24]. No empty spheres were necessary to achieve space filling. A total of 512 irreducible *k*-points were needed for Brillouin zone integrations using the tetrahedron method [28]. Self-consistency was achieved when the total energy change was smaller than 0.01 mRy (0.136 meV).

Acknowledgment

The FRM II is acknowledged for providing neutron beamtime on PGAA, and Lea Canella is acknowledged for assistance during the data acquisition. RH acknowledges support from the Helmholtz-University Young Investigator Group "Lattice Dynamics in Emerging Functional Materials". We also thank DFG for having funded this study.

References

[1] G.W. Wiener, J.A. Berger, J. Met 7 (1955) 360.
[2] S.K. Chen, S. Jin, T.H. Tiefel, Y.F. Hsieh, E.M. Gyorgy, D.W. Johnson Jr., J. Appl. Phys. 70 (1991) 6247.
[3] C. Guillard, H. Creveaux, C.R. Hebd, Seances Acad. Sci. 222 (1846) 1170.
[4] D. Andriamandroso, S. Matar, G. Demazeau, L. Fournès, IEEE Trans. Magn. 29 (1993) 2.
[5] B. Siberchicot, S.F. Matar, L. Fournès, G. Demazeau, P. Hagenmüller, J. Solid State Chem. 84 (1990) 10.
[6] S. Matar, L. Fournès, S. Chérubin-Jeannette, G. Demazeau, Eur. J. Solid State Inorg. Chem. 30 (1993) 871.
[7] A. Houben, J. Burghaus, R. Dronskowski, Chem. Mater. 21 (2009) 4332.
[8] J. Burghaus, M. Wessel, A. Houben, R. Dronskowski, Inorg. Chem. 49 (2010) 10148.

[9] A. Houben, P. Müller, J. von Appen, H. Lueken, R. Niewa, R. Dronskowski, Angew. Chem. Int. Ed. 44 (2005) 7212.
[10] L. Pauling, J. Am. Chem. Soc. 69 (1947) 542.
[11] G.L. Molnár, Handbook of Prompt Gamma Activation Analysis with Neutron Beams, Kluwer Academic Press, Dordrecht, Boston, London, 2004.
[12] O. Bartels, K.D. Becker, Z. Phys. Chem. 221 (2007) 1509.
[13] A. Houben, V. Sepelak, K.D. Becker, R. Dronskowski, Chem. Mater. 21 (2009) 784.
[14] R.P. Hermann, O. Tegus, E. Brück, K.H.J. Buschow, F.R. de Boer, G.J. Long, F. Grandjean, Phys. Rev. B 70 (2004) 214425.
[15] R. Hu, R.P. Hermann, F. Grandjean, Y. Lee, J.B. Warren, V.F. Mitrović, C. Petrovic, Phys. Rev. B 76 (2007) 224422.
[16] S. Matar, P. Mohn, G. Demazeau, B. Siberchicot, J. Phys. France 49 (1988) 1761.
[17] Q. Qi, K. O'Donnel, E. Touchais, J.M.D. Coey, Hyperfine Interact 94 (1994) 2067.
[18] E.C. Stoner, Proc. Roy. Soc. Lond. A 154 (1936) 656.
[19] E.C. Stoner, Proc. Roy. Soc. Lond. A 165 (1938) 372.
[20] J. Hubbard, Proc. Roy. Soc. Lond. A 276 (1963) 238.
[21] J. Kübler, Theory of Itinerant Electron Magnetism, Clarendon Press, Oxford, 2000.
[22] M.E. Elzain, A.A. Yousif, A.D. Al Rawas, A.M. Gismelseed, H. Widatallah, K. Bouziani, I. Al-Omari, Hyperfine Interact. 164 (2005) 3.
[23] O.K. Andersen, O. Jepsen, Phys. Rev. Lett. 53 (1984) 2571.
[24] O.K. Andersen, Phys. Rev. B 12 (1975) 3060.
[25] J. Korringa, Physica 13 (1947) 392.
[26] W. Kohn, N. Rostoker, Phys. Rev 94 (1954) 1111.
[27] G. Krier, O. Jepsen, A. Burkhardt, O.K. Andersen, TB-LMTO-ASA V4.7c, Max-Planck-Institut für Festkörperforschung, Stuttgart.
[28] P. Blöchl, O.K. Andersen, O. Jepsen, Phys. Rev. B 34 (1994) 16223.